2.0 AREA OF REVIEW AND CORRECTIVE ACTION PLAN
40 CFR 146.84

CLECO DIAMOND VAULT PROJECT

Facility Information

Facility name: DIAMOND VAULT

Facility contact: Sensitive, Confidential, or Privileged Information [redacted]

Well name: CLDV-IW4

Well location: RAPIDES PARISH, LOUISIANA
Sensitive, Confidential, or Privileged Information [redacted]

Table of Contents

2.0 AoR and Corrective Action Plan 6
2.1 Computational Modeling Approach (40 CFR 146.84 (a), (b)(1)) 6
2.1.1 Model Background 6
2.1.2 Site Geology and Hydrology 7
2.1.3 Model Domain 12
2.1.4 Porosity and Permeability 14
2.1.5 Constitutive Relationships and Other Rock Properties 20
2.1.6 Boundary Conditions 21
2.1.7 Initial Conditions 21
2.1.8 Operational Information 23
2.1.9 Fracture Pressure and Fracture Gradient 23
2.2 Computational Modeling Results (40 CFR 146.84 (c)(1), (g)) 24
2.2.1 Predictions of System Behavior 24
2.2.2 Model Calibration and Validation 34
2.3 AoR Delineation 44
2.3.1 Critical Pressure Calculations 44
2.3.2 AoR Delineation 44
2.4 Corrective Action (40 CFR 146.84 (b)(d)(e)) 45
2.4.1 Tabulation of Wells within the AoR 45
2.4.2 Wells Penetrating the Confining Zone 51
2.4.3 Plan for Site Access 51
2.4.4 Corrective Action Schedule (40 CFR 146.84 (e)) 51
2.5 Re-evaluation Schedule and Criteria 52
2.5.1 AoR Re-evaluation Cycle 52
2.5.2 Triggers for AoR Reevaluations Prior to the Next Scheduled Reevaluation (40 CFR 146.84 (f)) 54
2.6 References 56

List of Tables

Table 2-1: SEM domain information. 13

Table 2-2: Proportions (percent) of each facies type assigned by zone and depositional environment. 15

Table 2-3: Initial model conditions. 22

Table 2-4: Injection well operating details. 23

Table 2-5: Injection well pressure details. 24

Table 2-6: Input data used for critical pressure calculation. 44

Table 2-7: Tabulation of wells within the AoR. 49

Table 2-8: Wells penetrating the confining zone within the AoR and their measured depths. 51

Table 2-9: Changes in operations and site characterization that may trigger AoR re-evaluation. 55

Table 2-10: Observed changes in monitoring data that may trigger an AoR re-evaluation. 55

List of Figures

Figure 2-1: Depositional systems of the Gulf Coast during Carrizo Sandstone deposition. The Carrizo Fluvial Complex and the Rosita Delta were the primary sediment source for this formation (modified from Hackley, 2012). The Cleco Diamond Vault site location is denoted with yellow star. 8

Figure 2-2: Depositional systems of Louisiana during Wilcox deposition. A) The Holly Springs Delta and the Mississippi Embayment were the primary sediment source for this formation. The Cleco Diamond Vault site location is denoted with a yellow star (modified from Galloway, 1968), B) Paleo-reconstruction of the Paleocene period (60 million years ago) depicting the Holly Springs Delta in Eastern Louisiana, and C) Modern analog of a fluvial-deltaic system. 9

Figure 2-3: Depositional facies for fluvial-dominated deltas and their three main components: Flood Plain, Channel Axis, and Off-Axis Channel. 10

Figure 2-4: Example of interpreted depositional facies for the caprock and reservoir zones at the Cleco Diamond Vault site location for the Bentley Lumber-1 and Bentley Lumber-21 wells. ... 11

Figure 2-5: Map displaying main surface water bodies at the Cleco Diamond Vault site 12

Figure 2-6: Static Earth Model boundary at 16.5-miles by 19-miles and the Dynamic Reservoir Model boundary at 7.5 miles by 8 miles. Injection well locations shown in red, wells with data incorporated into the model shown in black. 13

Figure 2-7: Model Zones and corresponding vClay, Sp, and Resistivity logs. The Cane River acts as the confining unit, with the Wilcox 1 and Wilcox 2 targeted for injection. Cleco property outline shown at center of the grid. 14

Figure 2-8: Histograms of log porosity ranges by facies type showing correlative distributions for the clean sand, silty sand, silt, and shale facies. 15

Figure 2-9: Final (a) porosity and (b) permeability properties showing the effect of depositional constraints on spatial property distribution within the 3D geocellular model. 17

Figure 2-10: Porosity-Permeability cross-plot colored by facies showing the utilization of four different transforms applied by facies type. 18

Figure 2-11: Logs at the Bentley Lumber-3 well showing (left to right) vClay, stratigraphic zone, EOD, Facies, porosity, and permeability. There is a match between the model (blocky colors) and the log (black dashed line) for upscaled porosity and calculated permeability. 19

Figure 2-12: Relative Permeability Curves imported into dynamic reservoir model from Dismukes et al 2019. The blue curve represents relative permeability of water, and the red curves represents relative permeability of CO_2. 20

Figure 2-13: Calculated log salinity of the Wilcox 2 in the area in thousands of ppm, colored by unique well. 22

Figure 2-14: Map view of the DRM with zoomed well pad grid showing local grid refinement around injection wells (top), cross section of the model showing injection well (bottom). 25

Figure 2-15: CO_2 plume development around the CLDV-IW4 well at the Wilcox 1 formation, during injection period showing map view (left) and cross sectional view (right) of the CO_2 plume at 4, 8, and 12 years. 27

Figure 2-16: Post-injection CO_2 plume dynamics around the CLDV-IW4 well at the Wilcox 1 formation, showing map view (left), and cross sectional view of the CO_2 plume at 5, 10, and 50 years post-injection (right). 28

Figure 2-17: Cross sectional view of pressure front (using 110 psi cutoff) around the CLDV-IW4 well at the Wilcox 1 formation, 4, 8 and 12 years after injection. 29

Figure 2-18: Cross sectional view of pressure Front around the CLDV-IW4 well at the Wilcox 1 formation, (using 110 psi cutoff) at 2 and 5 years post injection. 30

Figure 2-1: Pressure time-series data during injection (12 years) and 50 years of post-injection period at depth of top perforation. 31

Figure 2-20: Development of combined pressure front (from 6 injection wells), and CO_2 plume after 4, 8 and 12 years of injection. 32

Figure 2-21: Development of combined pressure front (from 6 injection wells) and CO_2 plume 2 and 5 years after the end of injection. 33

Figure 2-22: Moles of CO_2 dissolved in brine during injection and post-injection period (blue). Moles of CO_2 residually trapped in brine during injection and post-injection period (red). 34

Figure 2-23: Comparison of the base case plume boundary after 12 years of injection (white solid line) versus sensitivity cases including 35,000 ppm salinity (dashed red line), 80,000 ppm salinity (dashed blue line), and multiple relative permeability curves (dashed black line)..... 35

Figure 2-24: Map view of plume movement during injection period with 35,000 ppm brine salinity (left) and cross sectional view (right) of the CO_2 plume at 4, 8, and 12 years. 37

Figure 2-25: Map view of post-injection plume dynamics with 35,000 ppm brine salinity (left), and cross sectional view (right) of the CO_2 plume at 5, 10, and 50 years post-injection. 38

Figure 2-26: Map view of plume movement during injection period with 80,000 ppm brine salinity (left), and cross sectional view of the CO_2 plume at 4, 8, and 12 years (right). 39

Figure 2-27: Map view of post-injection plume dynamics with 80,000 ppm brine salinity showing (left), and cross sectional view of the CO_2 plume at 5, 10, and 50 years post-injection (right). 40

Figure 2-28: Map view of plume movement during injection period with multiple relative permeability curves (left), and cross sectional view of the CO_2 plume at 4, 8, and 12 years (right). 42

Figure 2-29: Map view of post-injection plume dynamics with multiple relative permeability curves (top), and cross sectional view of the CO_2 plume at 5, 10, and 50 years post-injection (bottom)..... 43

Figure 2-30: Map showing the modeled Area of Review, existing wells, and proposed injection wells within the AoR. Well data is summarized in Table 2-7. 50

Figure 2-31: Workflow used to update the SEM and computational modeling. 53

2.0 AoR and Corrective Action Plan

This Area of Review (AoR) and Corrective Action Plan describes the computational modeling performed to derive the AoR and the corrective actions to be taken in response to changes in the AoR, in compliance with 40 CFR 146.84.

As described in the Project Narrative (Permit Section 1.0), the Cleco Power, LLC Diamond Vault project is proposed as a six injection well site. The computational model described below has been built to cover the area of all six wells. There is therefore a single static earth model (SEM) covering the whole project. Where appropriate, descriptions below refer to the whole project area; details describing injection well specific items are clearly defined.

A stratigraphic test well (STW) will be drilled at the site to characterize the subsurface within the AoR at the Diamond Vault site. Extensive wireline logging, coring, fluid sampling, and formation hydrogeologic testing will be performed in the STW well. The data will be incorporated into the SEM and dynamic reservoir models (DRM).

2.1 Computational Modeling Approach (40 CFR 146.84 (a), (b)(1))

2.1.1 Model Background

Computational modeling at the Cleco Diamond Vault Project site has been completed to delineate the plume size and shape, area of pressure buildup, and AoR for injected carbon dioxide (CO_2). A SEM named Cleco_SEM_1 was prepared by Battelle using the Schlumberger Petrel® modeling software. The SEM is a three-dimensional (3D) geocellular model that represents petrophysical properties within the stratigraphic formations intended for CO_2 storage, as well as the overlying confining layer. This type of model offers the best options for quantifying, visualizing, and simulating dynamic behavior through the subsurface geology at the site. By integrating multiple data types, the model represents the spatial distribution of available pore space and flow potential (permeability), enabling a data-driven estimation of CO_2 storage capacity. The SEM serves as the framework (in terms of delineating zones, surfaces, porosity, and permeability) for dynamic simulation of CO_2 injection.

Computational dynamic reservoir modeling to simulate CO_2 injection into the saline aquifer was completed by Battelle using the 3D multiphase flow simulator CMG-GEM version 2016 (CMG-GEM, 2016). In addition to the geological framework and associated properties imported from the SEM, parameters such as relative permeability, initial reservoir conditions, phase behavior, and well completion were added to the dynamic model for simulation. CMG-GEM is an equation-of-state based compositional simulator that models the phase behavior of brine and CO_2 plumes during the injection and post-injection stages of a project.

Aqueous, gaseous, and supercritical phases of CO_2 were accounted for in the computational model. Component transport equations, which describe the thermodynamic equilibrium between gaseous or supercritical with aqueous phases, were used in the compositional simulator to model CO_2 injection into the saline aquifer (Nghiem et al., 2004). The Peng-Robinson equation of state was used to model the fluid properties of the injected CO_2 in gaseous/supercritical phases (Peng and Robinson, 1976). The solubility of the injected CO_2 in brine is modeled as a phase equilibrium process, which is computed using Henry's law to estimate the fugacity of the gaseous and aqueous phases as functions of pressure and temperature (Li and Nghiem, 1986; Enick and Klara, 1990; Nghiem et al., 2009a). Additionally, the viscosity and density of the aqueous phase were calculated as functions of pressure, temperature, and salinity. Rowe and Chou (1970) equation was used to estimate aqueous phase density, and the Kestin et al. (1981) correlation was used to estimate the viscosity of the aqueous fluids.

2.1.2 Site Geology and Hydrology

Subsurface characterization at Cleco Diamond Vault benefited from abundant data which include 25 wells from across the region. These well logs supplied regional and local measurements of in-situ physical rock properties, such as gamma ray (lithology) and porosity at depths that captured the entirety of the target reservoir and caprock formations. Additionally, three two-dimensional (2D) seismic lines were licensed to further enhance the subsurface characterization at the Diamond Vault site. For more information regarding subsurface data available refer to Section 1.2 of the Project Narrative (Permit Section 1.0).

The confining zone for the Cleco Diamond Vault site is the Cane River Formation. This formation consists of brown clay, glauconitic marls, and distal shelf shales deposited on a regionally muddy shelf (Galloway et al., 2000). Below the Cane River is the Carrizo Sandstone. This formation is comprised of fine to coarse-grain sandstones that were fed by the Carrizo Fluvial Complex located between the Rio Grande and Houston Embayment (Figure 2-1). This fluvial system extended along the central and south Texas margin and developed into strike-elongate deposits of the wave-dominated Rosita Delta System as sediments reached the paleo-shelf margin (Ewing and Galloway, 2019). Over time, these sediments were diverted east towards the Mississippi axis and reworked into shore-zone and shelf systems. At the Cleco Diamond Vault site location, this sandstone is interpreted to be deposited in a sandy shore-zone system (Galloway et al., 2000).

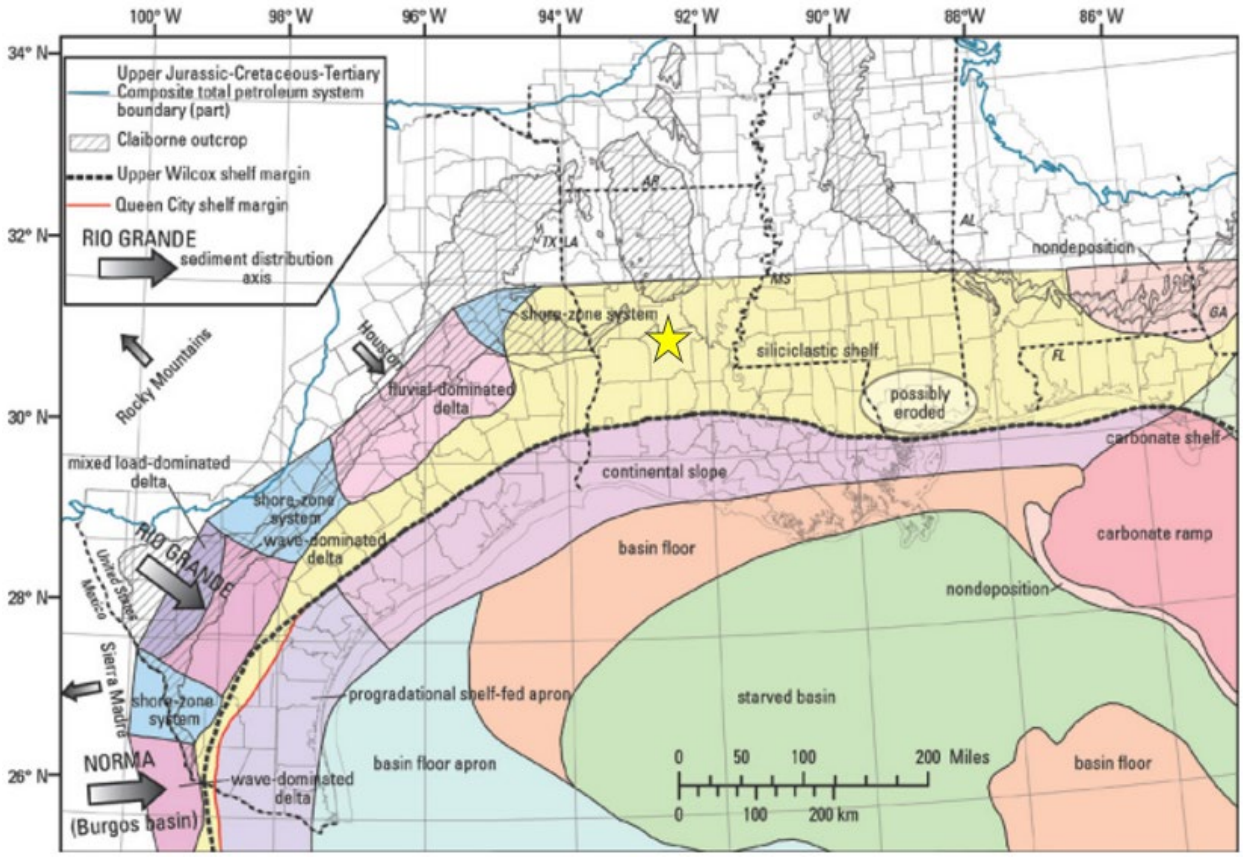

Figure 2-1: Depositional systems of the Gulf Coast during Carrizo Sandstone deposition. The Carrizo Fluvial Complex and the Rosita Delta were the primary sediment source for this formation (modified from Hackley, 2012). The Cleco Diamond Vault site location is denoted with yellow star.

The main target reservoir, the Wilcox Group (divided into Wilcox 1 and 2), is largely composed of sandstones and shales that were deposited in a fluvial-dominated delta system. The main sediment source during Wilcox deposition was the Holly Springs Delta, which was deposited from the north-northeast and later migrated eastward (Figure 2-2A and Figure 2-2B; Galloway, 1968; Galloway et al., 2000; Glawe, 1995; Tye et al., 1991). This delta system is characterized by lobate masses with arenaceous sediment centered along the axis of the Mississippi trough (Figure 2-2C; Ewing and Galloway, 2019; Galloway, 1968).

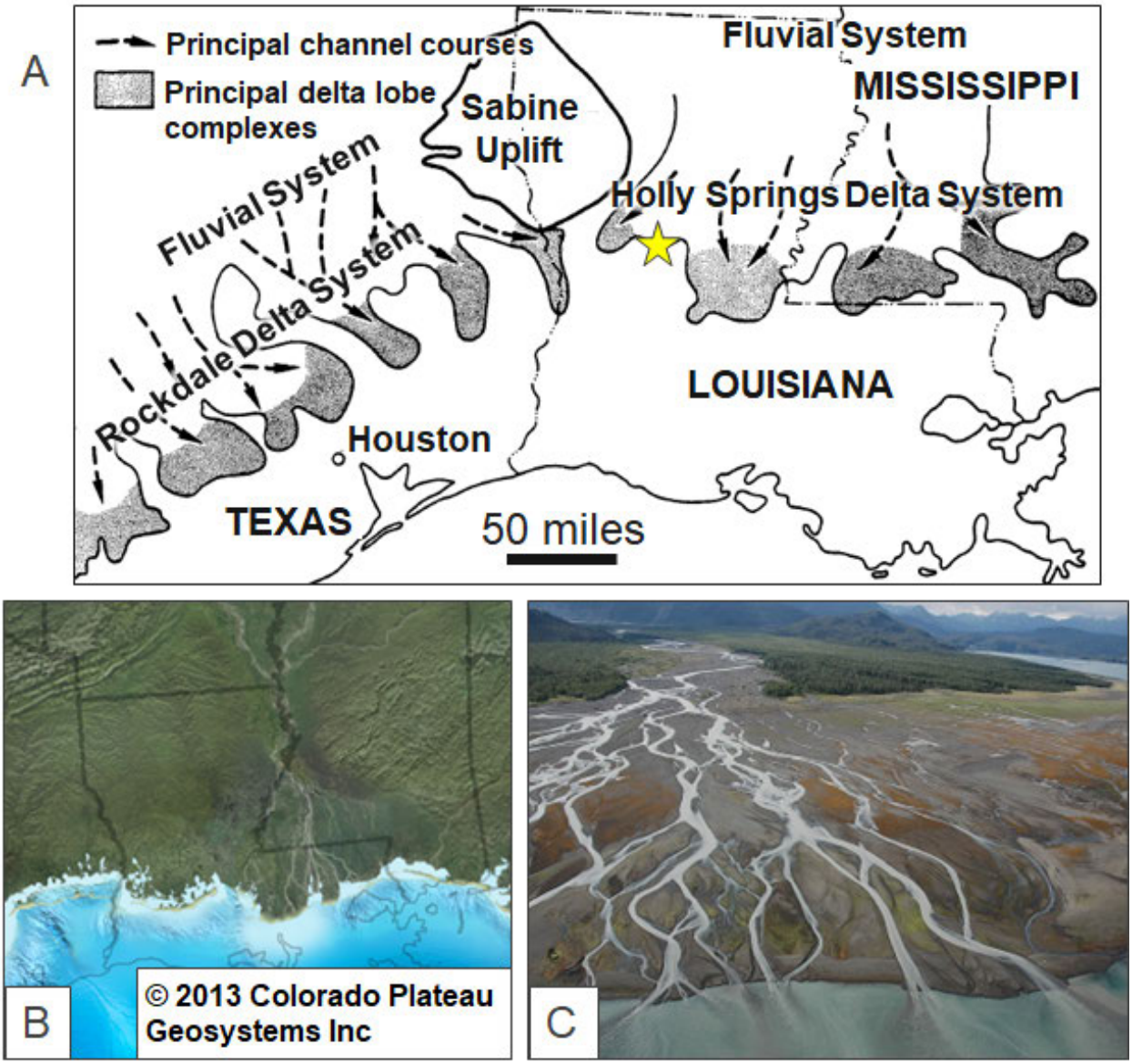

Figure 2-2: Depositional systems of Louisiana during Wilcox deposition. A) The Holly Springs Delta and the Mississippi Embayment were the primary sediment source for this formation. The Cleco Diamond Vault site location is denoted with a yellow star (modified from Galloway, 1968), B) Paleo-reconstruction of the Paleocene period (60 million years ago) depicting the Holly Springs Delta in Eastern Louisiana, and C) Modern analog of a fluvial-deltaic system.

Detailed depositional facies were assigned to each zone, which took into consideration the sediment source orientation and the broader environment of deposition (EOD) such as delta, coastal plain, and marine. The five main depositional facies identified were: 1) Marine, 2) Marginal Marine, 3) Flood Plain, 4) Channel Axis, and 5) Off-Axis Channel. These were defined based on literature reviews of the various EODs identified in these zones and analog work in

modern and ancient marine and fluvial-deltaic systems. The interpreted depositional facies for the Cane River confining zone is Marine (Hackley, 2012), as this is a regionally extensive transgressive shale that represents a rise in sea level and deep-water marine deposition. The Carrizo Sandstone reservoir is interpreted to have been deposited in a sandy shore-zone system (Hackley, 2012) and has been designated the depositional facies of Marginal Marine. This shore-zone system resulted in a laterally continuous, relatively clean sandstone package that makes up the Carrizo. The depositional facies for the Wilcox 1 and 2 were determined using literature examples for fluvial-deltaic systems (Ambrose, 2013; Galloway, 1968; Galloway et al., 2000; Glawe, 1995; Hackley, 2012; Tye et al., 1991). These were divided into three main components based on the character of the calculated volume of Clay (Vclay) log. These components are Flood Plain, Channel Axis, and Off-Axis Channel (Figure 2-3).

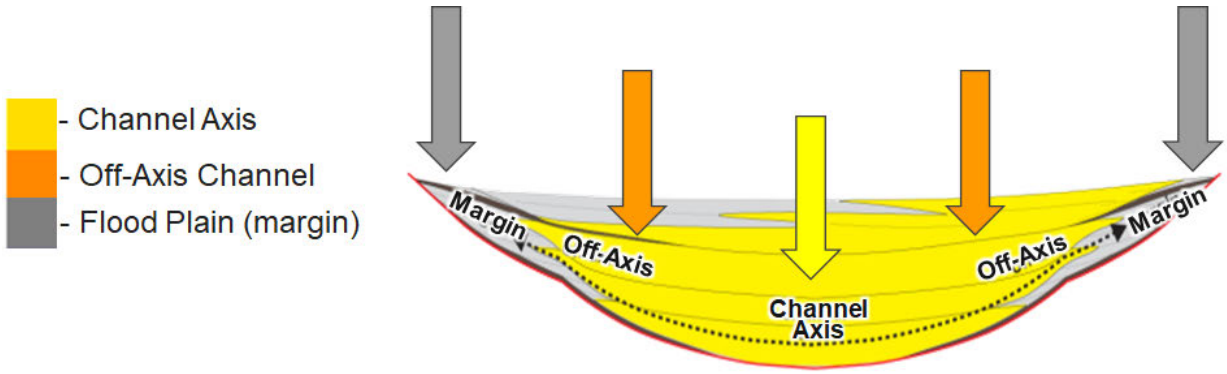

Figure 2-3: Depositional facies for fluvial-dominated deltas and their three main components: Flood Plain, Channel Axis, and Off-Axis Channel.

The Channel Axis facies is characterized by a low clay content volume and thick, clean sand packages, while the Off-Axis Channel facies has a relatively higher clay volume with thinner, interbedded sand packages. The last depositional facies described, the Flood Plain is characterized by a high clay volume and can vary in thickness. As shown in Figure 2-4, the Wilcox 2 contains a larger proportion of the Channel Axis facies than the Wilcox 1. This is a result of more sediment influx and prominent channels of the paleo-Holly Springs Delta present during deposition of the Wilcox 2, and the decline of this depocenter during deposition of the Wilcox 1 (Galloway et al., 2011; Milliken et al., 2018; Snedden et al., 2018).

Sensitive, Confidential, or Privileged Information

[redacted]

Figure 2-4: Example of interpreted depositional facies for the caprock and reservoir zones at the Cleco Diamond Vault site location for the Bentley Lumber-1 and Bentley Lumber-21 wells.

In terms of hydrology, the main body of water at the Cleco Diamond Vault site is Lake Rodemacher. This lake provides cooling water to the power plant and is open to the public; it is managed by Cleco Power, LLC and the Louisiana Department of Wildlife and Fisheries. The lake has a size of 3,070 acres (4.8 mi^2) and has an average depth of 9 ft. East of the site is the distributary Red River, which has a watershed that covers 65,590 mi^2 and flows southeast until it meets the Mississippi River (Benke and Cushing, 2005). The main water bodies at and near the Cleco Diamond Vault site location can be found on Figure 2-5.

Sensitive, Confidential, or Privileged Information

[redacted]

Figure 2-5: Map displaying main surface water bodies at the Cleco Diamond Vault site

2.1.3 Model Domain

Sensitive, Confidential, or Privileged Information

[redacted]

SEM domain information is summarized in Table 2-1 and a map view of both the SEM and DRM extent is shown in Figure 2-6.

Sensitive, Confidential, or Privileged Information

[redacted]

Sensitive, Confidential, or Privileged Information

[redacted]

Table 2-1: SEM domain information.

The SEM is subdivided into four internal zones based on observed responses seen in gamma ray, spontaneous potential (SP), and resistivity logs. These zones include the Cane River (confining unit), the Carrizo, and the Wilcox 1, and Wilcox 2 (injection intervals) as shown in Figure 2-7.

Sensitive, Confidential, or Privileged Information

[redacted]

2.1.4 Porosity and Permeability

The geology of the injection interval is characterized based on depositional environments and subsequent controls on sand-quality distribution and implied flow geometries. EODs were determined using paleogeographic information and well log analysis of 17 wells located within the SEM boundary.

EODs were defined on a zone-by-zone basis and incorporated into the model as channel-shaped objects for the fluvial deposition within the Wilcox 1 and Wilcox 2 formations. These objects provided a way to constrain facies distribution throughout the model, where environmental controls on the deposition of clean sand and shale components could be represented. As is shown in the results of the dynamic reservoir model (Figure 2-9), a strong north-south trend occurs in the plume for injection into the fluvial EOD influenced Wilcox 2 zone.

The facies used were defined with a clay fraction (vClay) log to separate the rock into three main types: clean sand, silty sand, silt, and shale, and compared to the resulting distribution of log porosity. The final vClay ranges used to determine facies type resulted in each facies having a unique normal or skewed-normal distribution of porosity values (Figure 2-8). These porosity ranges were utilized during the porosity property modeling process.

The facies themselves were distributed in the model using log-specified proportions within each EOD (Table 2-2). Notably, the channel axis EODs in the Wilcox 1 and Wilcox 2 zones contain the highest proportions of clean sands, while the Flood Plains contain only silt and shale. The Cane River, which serves as the caprock, is comprised almost entirely of shale.

Sensitive, Confidential, or Privileged Information

[redacted]

Figure 2-8: Histograms of log porosity ranges by facies type showing correlative distributions for the clean sand, silty sand, silt, and shale facies.

Sensitive, Confidential, or Privileged Information

[redacted]

Table 2-2: Proportions (percent) of each facies type assigned by zone and depositional environment.

The resulting porosity property (Figure 2-9a) was used as a direct input into the permeability property (Figure 2-9b), which was calculated in millidarcies (mD) using porosity-permeability transform functions derived from the Dutton & Loucks 2014 report on Reservoir Quality and Porosity-Permeability Trends in Onshore Wilcox Sandstones, Texas, and Louisiana Gulf Coast in the Gulf Coast Association of Geological Societies Journal. The porosity-permeability transforms are regionally derived parameters until site specific data are acquired at the STW

(Figure 2-10). The porosity-permeability functions were applied based on facies type, where each facies had a unique transform.

Results of the property models matches well log data (Figure 2-11) and reflect EOD-controlled anisotropy within the Wilcox 1 and Wilcox 2 zones, with strong north-south/northeast-southwest trends. The Carrizo shows a more east-west trended anisotropy, though the interpreted depositional environment provides less control on this directionality than that of the Wilcoxes. Results of simulation for the injection well are described in detail in Section 2.2.

Sensitive, Confidential, or Privileged Information

[redacted]

Figure 2-9: Final (a) porosity and (b) permeability properties showing the effect of depositional constraints on spatial property distribution within the 3D geocellular model.

Sensitive, Confidential, or Privileged Information

[redacted]

Figure 2-10: Porosity-Permeability cross-plot colored by facies showing the utilization of four different transforms applied by facies type.

Sensitive, Confidential, or Privileged Information

[redacted]

Figure 2-11: Logs at the Bentley Lumber-3 well showing (left to right) vClay, stratigraphic zone, EOD, Facies, porosity, and permeability. There is a match between the model (blocky colors) and the log (black dashed line) for upscaled porosity and calculated permeability.

2.1.5 Constitutive Relationships and Other Rock Properties

Relative permeability relationships served as the main constitutive relationships in the dynamic model. Relative permeability is an important input for describing dynamic behavior in reservoir simulators and it is a required property in the saturation equation describing multiphase flow in porous media. This flow property is represented as a saturation function and will significantly influence the simulated injection profiles. The relative permeability curves shown in Figure 2-12 were extracted from Krevor et al. (2012) following the methodology of Dismukes et al. (2019). The curves imported into the model were based on the steady state CO2-brine drainage relative permeability measurement for the Berea Sandstone core sample (Krevor et al., 2012). Dismukes et al. performed CO_2 storage simulation studies on the Bayou Sorrel and the Paradis Fields, located at close proximity to the South Louisiana industrial corridor. The curves shown below serve as sufficient input to the model which will be updated when core experimental data are available from the planned characterization well to reevaluate model results. The relative permeability and capillary pressure for the confining zone will also be measured. The model assumes rock compressibility of 4.74×10^{-6} 1/psi, using the Hall correlation relating rock compressibility to mean porosity of the Carrizo and Wilcox 1 and 2 formations within the boundaries of the reservoir dynamic model (Hall, 1953).

Sensitive, Confidential, or Privileged Information

[redacted]

Figure 2-12: Relative Permeability Curves imported into dynamic reservoir model from Dismukes et al 2019. The blue curve represents relative permeability of water, and the red curves represents relative permeability of CO_2.

2.1.6 Boundary Conditions

A volume multiplier of 100,000 was applied to grid cells at the edge of the model to represent an infinite open boundary condition as recommended by CMG-GEM (Nghiem et al., 2009). This is a reasonable assumption given that the target injection formations are correlatively extensive at different well locations in the SEM to account for the pressure plume propagation during injection simulations. The model's lower boundary is the base of the Wilcox 2 or top of the Midway group. While this surface is expected to have some topographical features, in general, it is assumed to dip to the south. Six injection wells were used toward the center of the model so that the CO_2 plume and pressure buildup would be far from the computational model boundary (7.5 mi × 8 mi) and the model would be able to capture the multiphase flow phenomena.

2.1.7 Initial Conditions

Sensitive, Confidential, or Privileged Information [redacted]

Sensitive, Confidential, or Privileged Information [redacted]

Sensitive, Confidential, or Privileged Information

[redacted]

Figure 2-13: Calculated log salinity of the Wilcox 2 in the area in thousands of ppm, colored by unique well.

Sensitive, Confidential, or Privileged Information

[redacted]

Table 2-3: Initial model conditions.

2.1.8 Operational Information

Details on the injection operation are presented in Table 2-4.

Sensitive, Confidential, or Privileged Information

[redacted]

Table 2-4: Injection well operating details.

2.1.9 Fracture Pressure and Fracture Gradient

Sensitive, Confidential, or Privileged Information [redacted]

Sensitive, Confidential, or Privileged Information [redacted]

The fracture pressure of the Cane River Shale and the Wilcox Sandstones will be measured in the STW using step rate and minifrac tests at multiple intervals as per the Pre-Operational Testing Plan (Permit Section 5.0). The maximum allowable bottomhole injection pressure while injecting will then be updated based on those field measurements if needed to reevaluate model results. This information is summarized in Table 2-5.

Sensitive, Confidential, or Privileged Information

[redacted]

Table 2-5: Injection well pressure details.

2.2 Computational Modeling Results (40 CFR 146.84 (c)(1), (g))

2.2.1 Predictions of System Behavior

A 3D multi-phase flow simulator (CMG-GEM, 2022) was used to model CO_2 injection, determine the CO_2 plume position, and pressure front at the end of the injection period and during the post-injection period. The model includes the target storage formations the Wilcox 1 and 2 and the Cane River confining zone shale formation. The geological model (SEM) that includes the permeability, porosity, and gridding of the model was imported from Petrel. The gas-water relative permeability relationship assigned to the model is described in Section 2.1.5.

The injection well is defined in the model with an s-shaped trajectory with a land-based surface location and injection zone located under Lake Rodemacher. The well will be vertical from when it enters the confining later to total depth. A cross-section view of the model at the wellbore location and a map view of the model are shown in Figure 2-14.

Sensitive, Confidential, or Privileged Information [redacted]

Sensitive, Confidential, or Privileged Information

[redacted]

Figure 2-14: Map view of the DRM with zoomed well pad grid showing local grid refinement around injection wells (top), cross section of the model showing injection well (bottom).

Sensitive, Confidential, or Privileged Information

[redacted]

Post-injection cross sections of the plume are shown in Figure 2-16. Map and cross-section views after 5, 10 and 50 years of the end of injection are shown, illustrating the CO_2 plume stability during the post-injection period. Although CO_2 might be experiencing geographic redistribution, the overall dimensions of the plume remain unchanged throughout the post injection period.

Sensitive, Confidential, or Privileged Information

[redacted]

Figure 2-15: CO_2 plume development around the CLDV-IW4 well at the Wilcox 1 formation, during injection period showing map view (left) and cross sectional view (right) of the CO_2 plume at 4, 8, and 12 years.

Sensitive, Confidential, or Privileged Information

[redacted]

Figure 2-16: Post-injection CO_2 plume dynamics around the CLDV-IW4 well at the Wilcox 1 formation, showing map view (left), and cross sectional view of the CO_2 plume at 5, 10, and 50 years post-injection (right).

Sensitive, Confidential, or Privileged Information

[redacted]

Sensitive, Confidential, or Privileged Information

[redacted]

Figure 2-17: Cross sectional view of pressure front (using 110 psi cutoff) around the CLDV-IW4 well at the Wilcox 1 formation, 4, 8 and 12 years after injection.

Sensitive, Confidential, or Privileged Information

[redacted]

Figure 2-18: Cross sectional view of pressure Front around the CLDV-IW4 well at the Wilcox 1 formation, (using 110 psi cutoff) at 2 and 5 years post injection.

Figure 2-19 shows the pressure time-series at the depth of the shallowest perforation. The pressure remains lower than the maximum injection pressure (90% fracture gradient), then declines rapidly after injection ceases.

Sensitive, Confidential, or Privileged Information

[redacted]

Figure 2-1: Pressure time-series data during injection (12 years) and 50 years of post-injection period at depth of top perforation.

Sensitive, Confidential, or Privileged Information

[redacted]

Figure 2-21 shows the pressure front associated with injection of all six wells and the CO_2 plume associated with injection in CLDV-IW4 after 2 and 5 years after the end of injection.

Sensitive, Confidential, or Privileged Information

[redacted]

Figure 2-20: Development of combined pressure front (from 6 injection wells), and CO_2 plume after 4, 8 and 12 years of injection.

Sensitive, Confidential, or Privileged Information

[redacted]

Figure 2-21: Development of combined pressure front (from 6 injection wells) and CO_2 plume 2 and 5 years after the end of injection.

Sensitive, Confidential, or Privileged Information

[redacted]

Sensitive, Confidential, or Privileged Information

[redacted]

Figure 2-22: Moles of CO_2 dissolved in brine during injection and post-injection period (blue). Moles of CO_2 residually trapped in brine during injection and post-injection period (red).

2.2.2 Model Calibration and Validation

The DRM described above will be calibrated using data acquired in the STW. Geological parameters (e.g., porosity, permeability), fluid flow data (e.g., relative permeability), and initial reservoir data (e.g., temperature, initial pressure gradient, fracture pressure gradient) will be used to calibrate the computational model.

In the absence of data from the STW and to address the range of uncertainty and demonstrate that impact on the DRM, three alternative DRM simulations were completed based on our current understanding of the range of variation of two uncertainty parameters: salinity and relative permeability. Each of these three scenarios is constrained to the same injection rate and only the uncertainty parameter is varied compared to the base case. They consist of 35,00 ppm salinity, 80,000 ppm salinity, and multiple relative permeability curves. Figure 2-23 illustrates the lateral extent of the base case at the end of 50 years of monitoring compared to that of each of the simulated uncertainties. Overall, the model suggests that there is only a slight chance of plume extent variation among the four scenarios (base case included). The following parts of this section will describe the plume in greater details including individual map views, cross sectional views, and post-injection plume dynamics.

Sensitive, Confidential, or Privileged Information

[redacted]

Figure 2-23: Comparison of the base case plume boundary after 12 years of injection (white solid line) versus sensitivity cases including 35,000 ppm salinity (dashed red line), 80,000 ppm salinity (dashed blue line), and multiple relative permeability curves (dashed black line)

Sensitive, Confidential, or Privileged Information

[redacted]

[redacted]

[redacted]

[redacted]

[redacted]

[redacted]

Sensitive, Confidential, or Privileged Information

[redacted]

Figure 2-24: Map view of plume movement during injection period with 35,000 ppm brine salinity (left) and cross sectional view (right) of the CO_2 plume at 4, 8, and 12 years.

Sensitive, Confidential, or Privileged Information

[redacted]

Figure 2-25: Map view of post-injection plume dynamics with 35,000 ppm brine salinity (left), and cross sectional view (right) of the CO_2 plume at 5, 10, and 50 years post-injection.

Sensitive, Confidential, or Privileged Information

[redacted]

Figure 2-26: Map view of plume movement during injection period with 80,000 ppm brine salinity (left), and cross sectional view of the CO_2 plume at 4, 8, and 12 years (right).

Sensitive, Confidential, or Privileged Information

[redacted]

Figure 2-27: Map view of post-injection plume dynamics with 80,000 ppm brine salinity showing (left), and cross sectional view of the CO_2 plume at 5, 10, and 50 years post-injection (right).

Since the base case DRM employs a single set of relative permeability curves for both shale and non-shale facies due to a lack of measured data, it is likely that in reality, the shale relative permeability can be lower performing than its non-shale counterparts in our base case. A set of relative permeability curves with higher residual water saturation for shale facies has been adopted to experiment whether the influence would be significant on the plume movement and total injection. Sensitive, Confidential, or Privileged Information [redacted]

[redacted]

[redacted]

Sensitive, Confidential, or Privileged Information

[redacted]

Figure 2-28: Map view of plume movement during injection period with multiple relative permeability curves (left), and cross sectional view of the CO_2 plume at 4, 8, and 12 years (right).

Sensitive, Confidential, or Privileged Information

[redacted]

Figure 2-29: Map view of post-injection plume dynamics with multiple relative permeability curves (top), and cross sectional view of the CO_2 plume at 5, 10, and 50 years post-injection (bottom).

2.3 AoR Delineation

2.3.1 Critical Pressure Calculations

Thornhill et al. (1982) defined the AoR as "the area around an injection well where, during injection, the [hydraulic] head of the formation fluid in the injection zone is equal to or greater than the hydraulic head of USDWs." In relation to the USDWs, the pressure increase threshold in the injection reservoir(ΔP_{if}) can be determined by:

$$\Delta P_{if} = P_u + \rho_i * g * (z_u - z_i) - P_i$$

where P_u is the initial fluid pressure in the USDW, ρ_i is the injection zone fluid density, g is the acceleration due to gravity, z_u is the representative elevation of the USDW, z_i is the representative elevation of the injection zone, and P_i is the initial pressure in the injection zone. Using the aforementioned equation and the input parameters in Table 2-6, the pressure increase threshold is calculated to be 110 psi. It is worth noting that the main assumption for this equation is the injection borehole is perforated only within the injection zone and the USDW.

Sensitive, Confidential, or Privileged Information

[redacted]

Table 2-6: Input data used for critical pressure calculation.

2.3.2 AoR Delineation

Sensitive, Confidential, or Privileged Information

[redacted]

2.4 Corrective Action (40 CFR 146.84 (b)(d)(e))

2.4.1 Tabulation of Wells within the AoR

Wells within the AoR were identified using well databases held by the Louisiana Department of Natural Resources (LDNR) and the United States Geological Survey (USGS). These include LDNR's SONRIS well database and the USGS's National Water Information System. Locations and information about shallow wells within the Cleco Diamond Vault property were determined by Cleco Power, LLC. There are 49 wells in the AoR, which are shown in Figure 2-30. These wells are detailed in Table 2-7 which includes the location, type, status of each well, and whether it penetrates the caprock.

Four wells in the AoR currently penetrate the confining zone in addition to the proposed wells related to the project. It is not believed that there are any deep historical wells in the area that have not been captured by these data sources, but this will be confirmed with a magnetometer survey.

Sensitive, Confidential, or Privileged Information

[redacted]

Sensitive, Confidential, or Privileged Information

[redacted]

Sensitive, Confidential, or Privileged Information

[redacted]

Sensitive, Confidential, or Privileged Information

[redacted]

Table 2-7: Tabulation of wells within the AoR.

Sensitive, Confidential, or Privileged Information

[redacted]

Figure 2-30: Map showing the modeled Area of Review, existing wells, and proposed injection wells within the AoR. Well data is summarized in Table 2-7.

2.4.2 Wells Penetrating the Confining Zone

Sensitive, Confidential, or Privileged Information

[redacted]

Sensitive, Confidential, or Privileged Information

[redacted]

Table 2-8: Wells penetrating the confining zone within the AoR and their measured depths.

2.4.3 Plan for Site Access

One of the wells penetrating the confining zone is located on Cleco Power, LLC property and therefore accessible for remediation. All appropriate access permissions will be acquired by Cleco Power, LLC, prior to remediation of the remaining three wells. The remediation plan will be presented to relevant landowners that is consistent with the Corrective Action Plan and will ensure protection of all USDWs.

2.4.4 Corrective Action Schedule (40 CFR 146.84 (e))

Any wells identified from the well search and magnetometer survey as penetrating to the depth of the proposed caprock, the Cane River shale formation, will be re-entered as follows:

1. Locate well, install wellhead, and rig up workover rig
2. Install and test blow out prevention equipment (BOPE)
3. Drill out surface plug and pressure test casing

4. Drill out show / USDW plug, clean out to base of Cane River caprock plus 150 ft, if possible
5. Place CO_2 resistive cement across from deepest part of well across both Cane River and Cook Mountain caprocks
6. Place USDW protection cement plugs as required

Cement plugs are being selected as the preferred isolation mechanism. The method of running casing to TD and pumping cement up the back side would be less effective as it adds a conduit for CO_2 to the surface. The work will be performed with a workover rig with capability tailored to clean out plug and abandonment (P&A) cement from existing holes. A tri-cone bit cleanout assembly will be utilized. The wellbores are reportedly vertical and are not expected to have significant doglegs.

2.5 Re-evaluation Schedule and Criteria

2.5.1 AoR Re-evaluation Cycle

Cleco Power will re-evaluate the above described AoR every five years during the injection and post-injection phases pursuant to 146.84 (e).

The workflow (procedures) for incorporating the new data into the models as the project progresses is detailed in Figure 2-31.

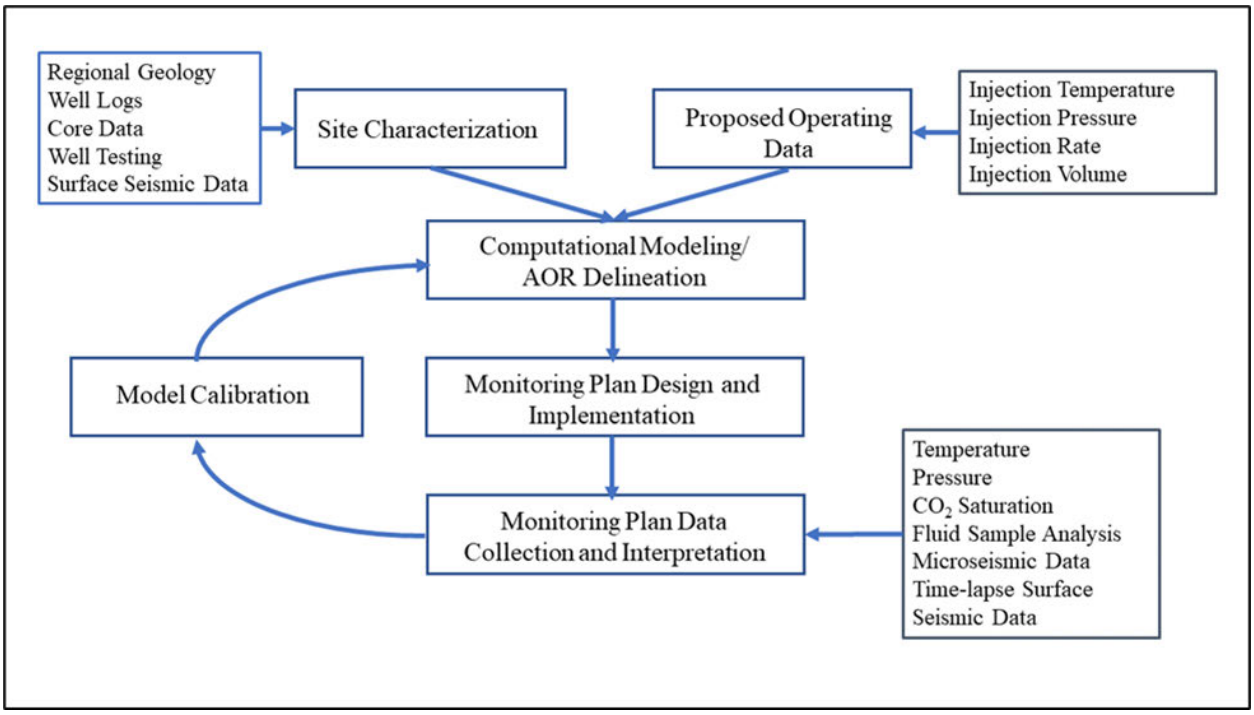

Figure 2-31: Workflow used to update the SEM and computational modeling.

With new data, model refinement is anticipated. The comparison of the original modeling with the updated modeling can take the form of several key evaluation metrics. This includes a comparison of:

- Changes to the static CO_2 resource estimate
- Differences in CO_2 plume geometry and volume
- Changes in pressure response

Any updates to the AOR will include an assessment of any additional wells that might be in the re-evaluated AoR that may need corrective action as well as an amended AoR and corrective action plan (40 CFR 146.84 (e)).

Once the injection phase of the project commences, both operational and verification monitoring data will be used to calibrate and update the computational model. Figure 2-31 illustrates the workflow and data inputs used to inform and calibrate the computational modeling. Operational monitoring data will be recorded on a continuous basis through the injection phase of the project. Pressure sensors located in the deep monitoring well will be retrieved on a quarterly basis for data download. In addition, pulsed neutron logs will be acquired in the deep monitoring well on a yearly basis to monitor CO_2 saturations along the well bores. The pressure and CO_2 saturation data from the deep monitoring well will be particularly useful in calibrating the computational model, as it will provide data on how the pressure plume is propagating through the injection zone away from the injection well. Computational model updates are also expected to occur

when the time-lapse borehole seismic data are acquired. For more details on the Testing and Monitoring Plan and schedule refer to Permit Section 7.

The computational modeling will be updated with the downhole pressure and operational monitoring data on a quarterly basis for the first year of injection. If the system stabilizes, model updates will be scaled back to semi-annual updates to coincide with EPA reporting requirements. Any significant divergence of the monitoring data from the model predictions will be identified during the regular model updates and investigated. Model calibration with early monitoring data is expected to improve model predictions over the course of injection. It should be noted that model history-matching and calibration are not expected to trigger AoR reevaluations on a regular basis.

2.5.2 Triggers for AoR Reevaluations Prior to the Next Scheduled Reevaluation (40 CFR 146.84 (f))

The AoR will be updated on a 5-year schedule. However, Cleco Power, LLC will discuss any events that could impact the AoR with the UIC Director to determine if an AoR re-evaluation is required. If an unscheduled re-evaluation is triggered, Cleco Power, LLC will perform the steps described at the beginning of this section of this Plan. A report will be submitted to the UIC Director within 90 days of the AoR re-evaluation.

Monitoring and operational conditions that may warrant a re-evaluation of the AoR include:

- Changes in site operations that might alter the model predictions or the AoR delineation
- Site characterization data that may significantly change the computational model predictions and delineated AoR
- Monitoring results that indicate that the areal extent of the CO_2 plume or pressure front differ significantly from the model predictions
- Monitoring results indicate that the CO_2 has migrated beyond the confining zone

Table 2-9 details the operational changes and site characterization data that may warrant a reevaluation of the AoR. Table 2-10 specifies the observed changes and monitoring technologies that may trigger a re-evaluation of the AoR. Refer to the Testing and Monitoring Plan for more details on the proposed monitoring technologies for the project (Permit Section 7).

Area of Change	Variable
Operational Changes	• Increase in number of Class VI injection wells injecting in project area • Increase in CO_2 injection rates or volumes • Injection pressures more than the maximum allowable injection pressure for the project
Site Characterization Data	• Identification of a potential conduit for CO_2 or brine migration through the confining zone • Further characterization of storage formation heterogeneity that significantly effects CO_2 and pressure plume development

Table 2-9: Changes in operations and site characterization that may trigger AoR re-evaluation.

Observed Change	Monitoring Technology
Significantly larger pressure increases in the injection formation in the monitor well than were predicted by the model	Pressure sensors
Early breakthrough of CO_2 at the monitor well	Fluid sampling Pulsed neutron logging
CO_2 plume expands much faster than predicted by model	Time-lapse surface seismic data
Sustained pressure increases observed in above confining zone (ACZ) monitoring intervals	Pressure sensors
Geochemical changes in the ACZ monitoring intervals indicate potential CO_2 or brine migrations above the confining layer	Fluid sampling
CO_2 accumulations identified in the ACZ intervals	Pulsed neutron logging Time-lapse surface seismic data

Table 2-10: Observed changes in monitoring data that may trigger an AoR re-evaluation.

If the re-evaluated AoR is substantially different from the previous AoR, the project will identify all active and abandoned wells that penetrate the confining zone in the re-evaluated AoR and will perform corrective actions on those wells (40 CFR 146.84 (e)). As needed, all other plans, such as the Emergency and Remedial Response Plan, will be revised to account for the re-evaluated AoR and those plans will be submitted to the UIC Director for review and approval (40 CFR 146.84 (f)).

Note that seismic events are covered under the Emergency and Remedial Response Plan. A tiered approach to responding to seismic events will be based on magnitude and location. A notification procedure is provided in that plan.

2.6 References

Ambrose, W. A., Loucks, R. G., and Dutton, S. P., 2013, Depositional Systems and Controls on Reservoir Quality (Determined from Core Data) in Deeply Buried Tertiary Strata in the Texas-Louisiana Gulf of Mexico: The University of Texas at Austin, Bureau of Economic Geology, Report of Investigations No. 278, 80 p

Benke, Arthur, and Cushing Colbert, 2005, River of North America. Academic Press. p. 1144.

Carlson, D., & Van Biersel, T. (2009). Dependence of the Wilcox aquifer water chemistry on stratigraphy, spatial distribution, and proximity to lignite in Southern Caddo Parish, Louisiana.

CMG-GEM. Advance compositional and GHG reservoir simulator user's guide. Calgary, Alberta 2016.

Dismukes, David E, Zeidouni, Mehdi, Zulqarnain, Muhammad, Hughes, Richard, Hall, Keith, Snyder, Brian, Layne, Michael, Lorenzo, Juan M, John, Chacko, & Harder, Brian. 2019. Integrated Carbon Capture and Storage in the Louisiana Chemical Corridor. United States. https://doi.org/10.2172/1526406

Dutton, S. P., & Loucks, R. G. (2014). Reservoir quality and porosity-permeability trends in onshore Wilcox sandstones, Texas and Louisiana Gulf Coast: Application to deep Wilcox plays, offshore Gulf of Mexico

Enick RM, Klara SM. CO2 solubility in water and brine under reservoir conditions. Chemical Engineering Communications 1990;90(1):23-33.

Ewing, T. E., & Galloway, W. E. (2019). Evolution of the northern Gulf of Mexico sedimentary basin. In The sedimentary basins of the United States and Canada (pp. 627-694). Elsevier

Galloway, W. E., Ganey-Curry, P. E., Li, X., and Buffler, R. T., 2000, Cenozoic Depositional History of the Gulf of Mexico Basin. AAPG Bulletin, 84 (11), 1743-1774 p.

Galloway, W. E., 1968, Depositional Systems of the Lower Wilcox Group, North-Central Gulf Coast Basin: Gulf Coast Association of Geological Societies Transactions, v. 18, 275–289 p.

Glawe, L. N. (1995). Paleoenvironments and Sequences of Subsurface Paleocene Wilcox in Sabine Parish, Louisiana.

Hackley, P. C., 2012, Geologic Assessment of Undiscovered Conventional Oil and Gas Resources—Middle Eocene Claiborne Group, United States part of the Gulf of Mexico Basin, U.S. Geological Survey Open-File Report 1144, 1-87 p.

Hall HN. Compressibility of reservoir rocks. Journal of Petroleum Technology 1953;5(01):17-9.

Kestin J, Khalifa HE, Correia RJ. Tables of the dynamic and kinematic viscosity of aqueous NaCl solutions in the temperature range 20–150 C and the pressure range 0.1–35 MPa. Journal of physical and chemical reference data 1981;10(1):71-88

Krevor SC, Pini R, Zuo L, Benson SM. Relative permeability and trapping of CO_2 and water in sandstone rocks at reservoir conditions. Water resources research 2012;48(2).

Land CS. Calculation of imbibition relative permeability for two-and three-phase flow from rock properties. Society of Petroleum Engineers Journal 1968;8(02):149-56.

Li YK, Nghiem LX. Phase equilibria of oil, gas and water/brine mixtures from a cubic equation of state and Henry's law. The Canadian Journal of Chemical Engineering 1986;64(3):486-96.

Milliken, K. T., Blum, M. D., Snedden, J. W., & Galloway, W. E. (2018). Application of fluvial scaling relationships to reconstruct drainage-basin evolution and sediment routing for the Cretaceous and Paleocene of the Gulf of Mexico. Geosphere, 14(2), 749-767

Bosshart, Nicholas W., Pekot, Lawrence J., Wildgust, Neil, Gorecki, Charles D., Torres, Jose A., Jin, Lu, Ge, Jun, Jin, Tao, Heebink, Loreal V., Kurz, Marc D., Dalkhas, Chantsalmaa, Peck, Wesley D., and Burnison, Shaughn A.. 2018. "Best Practices for Modeling and Simulation of CO2 Storage". United States. https://doi.org/10.2172/1874457. https://www.osti.gov/servlets/purl/1874457.

Nghiem L, Sammon P, Grabenstetter J, Ohkuma H. Modeling CO_2 storage in aquifers with a fully-coupled geochemical EOS compositional simulator. SPE/DOE symposium on improved oil recovery: Society of Petroleum Engineers; 2004

Nghiem L, Shrivastava V, Tran D, Kohse B, Hassam M, Yang C. Simulation of CO_2 storage in saline aquifers. SPE/EAGE Reservoir Characterization & Simulation Conference: European Association of Geoscientists & Engineers; 2009. p. cp-170-00063.

Peng, D.Y, Robinson, D.B., 1976, A New Two-Constant Equation of State Industrial & Engineering Chemistry Fundamentals 1976 15 (1), 59-64 DOI: 10.1021/i160057a011

Pettijohn, R. A., Weiss, J. S., and Williamson, A. K., 1988, Distribution of Dissolved-Solids Concentrations and Temperature in Ground Water of the Gulf Coast Aquifer Systems, South-Central United States, U.S. Geological Survey Water-Resources Investigations Report 88-4082

Pitman, J.K., Rowan, E., 2012. Temperature and Petroleum Generation History of the Wilcox Formation, Louisiana. U.S. Geological Survey, Reston.

Raziperchikolaee S, Alvarado V, Yin S. Effect of hydraulic fracturing on long-term storage of CO2 in stimulated saline aquifers. Applied energy 2013;102:1091-104.

Rowe, A.M. and Chou, J.C.S., "Pressure-Volume-Temperature-Concentration Relation of Aqueous NaCl Solutions", J. Chem. Eng. Data, Vol. 15, (1970), pp. 61-66

Snedden, J. W., Galloway, W. E., Milliken, K. T., Xu, J., Whiteaker, T., & Blum, M. D. (2018). Validation of empirical source-to-sink scaling relationships in a continental-scale system: The Gulf of Mexico basin Cenozoic record. Geosphere, 14(2), 768-784

Thornhill, J.T., Short, T.E., & Silka L. 1982. Application of the Area of Review Concept. Ground Water, 20:32-38.

Tye, R. S., Moslow, T. F., Kimbrell, W. C., & Wheeler, C. W. (1991). Lithostratigraphy and production characteristics of the Wilcox Group (Paleocene–Eocene) in central Louisiana. AAPG bulletin, 75(11), 1675-1713.

Zulqarnain, Muhammad , Zeidouni, Mehdi , and Richard G. Hughes. "Static and Dynamic CO_2 Storage Capacity Estimates of a Potential CO2 Geological Sequestration Site in Louisiana Chemical Corridor." Paper presented at the Carbon Management Technology Conference, Houston, Texas, USA, July 2017. doi: https://doi.org/10.7122/486020-MS